AGU PUBLICATIONS

Geophysical Research Letters

RESEARCH LETTER
10.1002/2018GL077076

Key Points:
- Longitudinal-seasonal-local time dependence of CEJ is delineated from 10 years of CHAMP satellite observations in a climatological sense
- Role of DE3 tide in causing the CEJ variabilities in seasonal time scales is brought out
- Results discussed in the context of available information are based on ground- and satellite-based observations

Correspondence to:
S. Gurubaran,
gurubara@iigs.iigm.res.in

Citation:
Singh, D., Gurubaran, S., & He, M. (2018). Evidence for the influence of DE3 tide on the occurrence of equatorial counterelectrojet. *Geophysical Research Letters*, *45*, 2145–2150. https://doi.org/10.1002/2018GL077076

Received 8 JAN 2018
Accepted 13 FEB 2018
Accepted article online 20 FEB 2018
Published online 8 MAR 2018

Evidence for the Influence of DE3 Tide on the Occurrence of Equatorial Counterelectrojet

Dupinder Singh[1], S. Gurubaran[1], and Maosheng He[2]

[1]Indian Institute of Geomagnetism, Navi Mumbai, India, [2]Leibnitz Institute of Atmospheric Physics, Rostock University, Kühlungsborn, Germany

Abstract The long-term Challenging Minisatellite Payload magnetometer data are analyzed to derive the equatorial counterelectrojet (CEJ) signatures globally over a range of local times. The resultant local time-longitude map of CEJ occurrence rate shows a strong influence of the diurnal eastward propagating wave number 3 (DE3) nonmigrating tide during July–September months. DE3 is also shown to account for the reduction of CEJ occurrence at certain longitudes. These aspects of DE3 tide-CEJ relationship have implications for understanding the seasonal and longitudinal variations of CEJ. Observations of zonal winds from the Thermosphere Ionosphere Mesosphere Energetics and Dynamics (TIMED) Doppler Interferometer instrument on board the TIMED satellite are used to establish these findings.

1. Introduction

The equatorial *E* region of the ionosphere supports an intense current system called the equatorial electrojet (EEJ) owing to the unique geometry of the Earth's magnetic field (see Yamazaki & Maute, 2017, for a recent review on Sq and EEJ current systems). The EEJ flows eastward (westward) during the day (night) concentrated within ±3° centered at the dip equator. The counterelectrojet (CEJ) refers to the reversal of EEJ from its usual eastward direction to westward direction during the daytime. The CEJ occurrence is pronounced in the morning and afternoon hours (Rastogi, 1974). Though the word "counterelectrojet" was coined five decades ago, identification of the underlying mechanism, however, remains elusive. There is little knowledge about the combined role of various drivers of the electric field responsible for CEJ, which altogether can explain the longitudinal, latitudinal, local time (LT), and seasonal dependence of CEJ.

Much of our understanding of CEJ so far came from extensive ground-based geomagnetic field observations from dip equatorial stations (Gurubaran, 2002; Marriott et al., 1979; Mayaud, 1977; Rastogi, 1974; Vichare & Rajaram, 2011). However, the number of equatorial sites that host magnetometers is quite small, and thus, the longitudinal coverage of the studies attempted has been somewhat limited. Large areas of the globe in the equatorial belt remain unexplored. In recent years, a few of the studies pursued with satellite data have provided newer insights of the global behavior of CEJ (McCreadie, 2005; Vichare & Rajaram, 2011).

Modeling efforts in the past were able to reproduce the westward electric field responsible for CEJ by invoking a certain combination of tidal modes (Hanuise et al., 1983; Marriott et al., 1979). However, the tidal phases required to produce the best fit to the experimental data were quite different from the observed tidal phases (Hanuise et al., 1983). Moreover, semidiurnal tides in the upper mesosphere were found to be enhanced during the time of CEJ occurrence (Somayajulu, 1988; Sridharan et al., 2002). A shift in the LT occurrence of CEJ with lunar phase suggested a connection between lunar tides and CEJ (Onwumechili & Akasofu, 1972; Rastogi, 1974). However, such a shift in the occurrence time of CEJ was not always consistent from one event to the other (e.g., Rangarajan & Rastogi, 1993; Reddy, 1981). As will be argued later, a single tidal mode of lunar or solar origin or both cannot account for all variabilities of CEJ, as their drivers have considerable seasonal dependence. Some authors suggested that shears in local winds could also modulate the occurrence of CEJ (Raghavarao & Anandarao, 1980). The other agencies known to induce temporal variability in the occurrence of CEJ were the modulation by the east/west phase of the stratospheric quasi-biennial oscillation (e.g. Chen et al., 1995), solar cycle activity (Marriott et al., 1979; Mayaud, 1977), enhanced planetary wave activity (Vineeth et al., 2007), sudden stratospheric warming (Stening et al., 1996), and lunar tides (Fejer et al., 2010).

In this work we focus on the afternoon CEJ (henceforth referred to as simply CEJ), as the tidal signatures are less clear in the morning CEJ. We first retrieve the longitudinal, LT, and seasonal variabilities of the CEJ from

Challenging Minisatellite Payload (CHAMP) magnetic field observations. As was done in an earlier work (Singh & Gurubaran, 2017), Thermosphere Ionosphere Mesosphere Energetics and Dynamics (TIMED) Doppler Interferometer (TIDI) data were analyzed for the same period to delineate the spatiotemporal climatologies of dominant tidal modes. When ordered in longitude-LT frame, the nonmigrating tide of diurnal eastward propagating wave number 3 (or DE3 tide as is known) reveals a climatological behavior very similar to that of the CEJ suggesting that much of the variability of CEJ occurrence can be ascribed to DE3.

2. Data and Method of Analysis

The method to retrieve EEJ/CEJ signatures from CHAMP magnetic field data follows that described by Lühr et al. (2004). The data chosen were the vector magnetometer data for the period 2001–2010. We consider daytime orbits (6–18 LT) during geomagnetic quiet times characterized by Kp less than or equal to 3. A total of 27,140 daytime passes is analyzed. For calculating the scalar residuals, the quiet time external and internal fields are removed by using the CHAMP, Oersted, and SAC-C version 6 model (Finlay et al., 2016). The solar quiet (Sq) currents are subtracted by fitting a fourth-degree polynomial to the latitude profile of the residuals (Lühr & Maus, 2006). While fitting the polynomial, the region around ±14° centered at the dip equator is masked so as not to affect the EEJ/CEJ signal. The scalar residuals are then inverted to produce current densities by application of Biot-Savart law to a simple current line model. This current line model consisted of 81 infinite current lines centered at the dip equator lying at an altitude of 108 km. As we are only interested in the variation and direction of the current, this simple current line model would suffice, though it underestimates the magnitude of the current density. The procedure for least square fitting includes a constraint that minimizes the second-order differences between current lines.

We use TIDI wind observations on board the TIMED mission for the period 2004–2014. The DE3 tidal amplitudes and phases corresponding to an altitude of 105 km are retrieved by grouping the data into 60 day windows and subjecting the data to a two-dimensional least square fitting. The climatological DE3 tidal amplitudes are calculated by applying vector addition over multiple years. Details of the methodology adopted herein can be found in Singh and Gurubaran (2017). The earlier work by Lühr and Manoj (2013) showed the tidal modulation of EEJ, whereas we focus on the modulation of CEJ.

3. Results

It has been recognized that the DE3 tide is a diurnal Kelvin wave (Forbes et al., 2003), primarily generated by the latent heating associated with deep tropical convection (Hagan & Forbes, 2002). This tidal mode has a stronger zonal component and a weaker meridional component. Among upward propagating tidal modes, DE3 has a larger vertical wavelength allowing it to penetrate deep into the ionosphere (Forbes et al., 2014; Hagan et al., 2007). DE3 controls the electrodynamics of the equatorial *E* region during the months when it is stronger (e.g., He et al., 2011; Wan et al., 2010). Immel et al. (2006) ascertained that the four-peak structure observed in the *F* region of the ionosphere is related to the nonmigrating tides of tropospheric origin. Further, the observed latitude structure of the DE3 tide in the zonal wind is such that it maximizes away from the geographic equator in the Southern Hemisphere (see Figure 3d of Singh & Gurubaran, 2017). As the geographic latitude of the dip equator changes with longitude, the DE3 winds as seen by the dip equator will also vary along the longitude. For longitudes where the dip equator lies to the south of the geographic equator, the DE3 winds would be stronger. This may have implications for the longitudinal dependence of CEJ occurrence as we explore below.

Figure 1 depicts the occurrence pattern of CEJ plotted in longitude-LT frame for the four groups of months, namely, January–March, April–June, July–September, and October–December. The blue dashed curve shows the geographic latitude of the dip equator in 2005 as a function of geographic longitude referring to the International Geomagnetic Reference Field-12 model. Each red circle represents a CEJ event with its size indicating the amplitude of CEJ.

The tilted red solid lines in Figure 1 are the zero-wind speed contours of climatological DE3 zonal winds at 105 km as derived from the TIDI zonal wind data, which outline the diurnal phase variation of DE3. The shaded (unshaded) portions in each of the panels represent westward (eastward) wind regimes. As can be appreciated from Figure 1, DE3 produces a wave number 4 structure in LT in the relevant parameters.

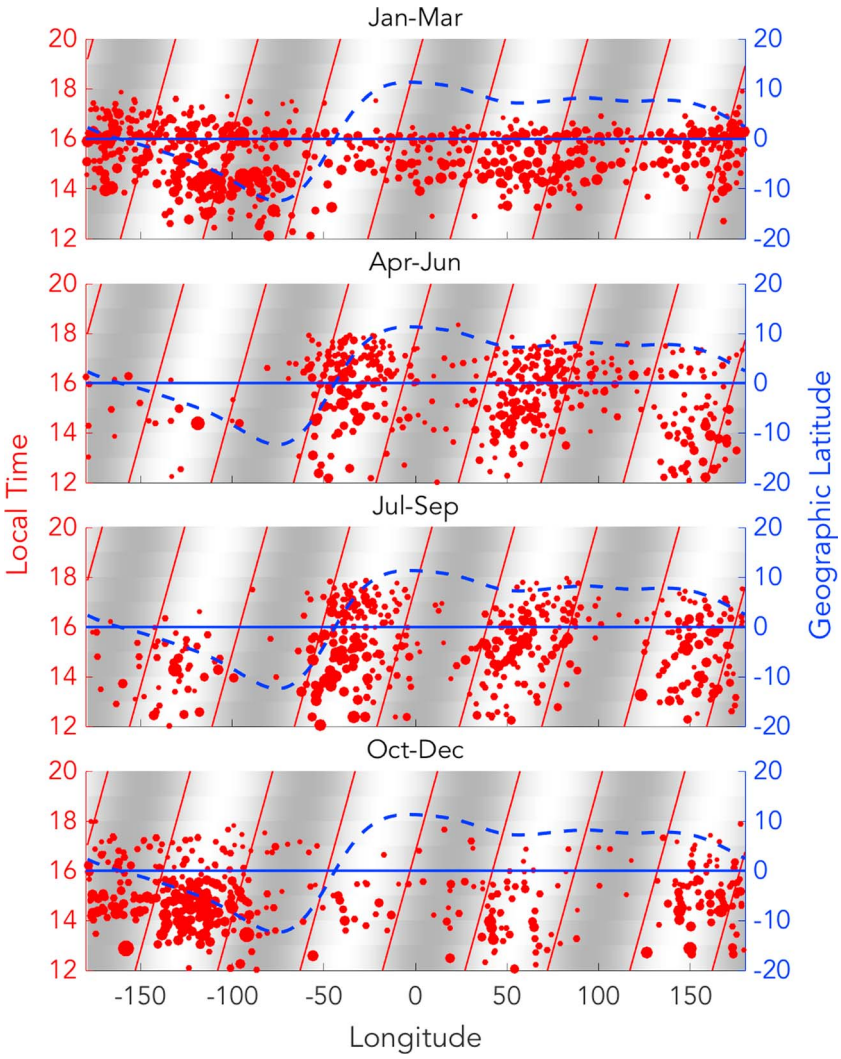

Figure 1. The afternoon counterelectrojet occurrence derived from Challenging Minisatellite Payload observations as a function of longitude and local time. The dashed line represents the dip equator as of year 2005. The vertical tilted solid lines are the DE3 zero-wind lines as derived from Thermosphere Ionosphere Mesosphere Energetics and Dynamics Doppler Interferometer observations for an altitude of 105 km. The horizontal line represents the location of the geographic equator.

There are a couple of remarkable features in Figure 1. The DE3 amplitude is known to be largest during the July–September period (He et al., 2010, 2011; Oberheide & Forbes, 2008). During these months of the year, we notice a shift in the CEJ occurrence longitude with LT, which is in excellent agreement with the tilt of the DE3 zero-wind lines at 105 km. It is evident that in a climatological sense, CEJs are more frequent when the DE3 winds are eastward. Moreover, the CEJ occurrence pattern is alternately spaced and there are longitude bands where CEJ is very frequent and immediately next to those bands the CEJ is less frequent. We refer to the latter longitude-LT zones as CEJ shadow zones. This pattern, however, appears to be less prominent for the western longitudes between ~−150° and ~−100°, which could partly arise from the offset between the geographic and geomagnetic equators in those longitudes. A similar feature of the CEJs appearing in alternate bands aligned with the DE3 zero-wind lines can be seen for the April–June period as well when DE3 has moderate amplitudes. CEJs are less frequent in the western longitudes during these months as well.

The contribution of other tides to the observed CEJ wave number 4 like occurrence pattern cannot be ruled out during these months. DE2 tide has a large vertical wavelength (Truskowski et al., 2014), though with a considerably reduced amplitude (Pedatella et al., 2008). When DE2 is incorporated in the analysis along

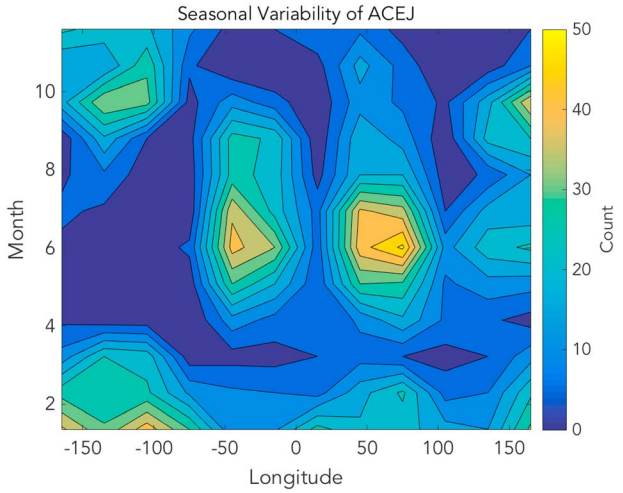

Figure 2. The number of counterelectrojet (CEJ) occurrences as a function of season and longitude as retrieved from Challenging Minisatellite Payload.

with DE3, we immediately notice a weakening of eastward winds in the −150° to −100° longitudes during April–June months, though the zero-wind lines remained unaltered (not shown here). This suggests a possible role of DE2 tide in modulating the CEJ longitude-LT occurrence pattern.

While DE3 dominates in modulating the longitude-LT behavior of CEJ occurrences during July–September when it exhibits enhanced activity, other tidal modes are expected to contribute to CEJ during other months. For example, the wave number 1 like pattern in the occurrence of CEJ during October–December months (Figure 1d) matches with the phase of the DW2 tide in such a manner that the CEJ occurrence longitude zones tend to fall within the eastward wind regimes of DW2.

In Figure 2 we show the seasonal variability of CEJ occurrence rate for various longitudes. The CEJ occurrences are depicted in 30° longitude bins for different months. The longitudinally dependent DE3 modulation of the CEJ occurrence is clearly evident in Figure 2 with four maxima extended from July to September. This pattern, however, is somewhat distorted if we take into account the shift in the maxima toward later months in the westernmost longitudes. The pattern for other months of the year is very different, and other tidal modes are expected to contribute to the observed pattern besides DE3 during those months. Surprisingly, the DE3-like wave number 4 pattern in CEJ occurrence and its seasonal dependence have not been reported earlier perhaps because it is hidden in the seasonal variation of CEJ occurrence any station sees.

While noting greater CEJ occurrences in longitude zones where DE3 winds are eastward (Figure 1), we draw attention to an earlier work by Yamazaki et al. (2014). Making use of the Thermosphere-Ionosphere-Mesosphere Electrodynamics general circulation model simulations with appropriate lower atmospheric forcing, this study suggests the day-to-day variability of the zonal winds at 100–120 km altitudes near the geomagnetic equator to be a potential source of the corresponding variability of the EEJ. In particular, it turns out from this study that an eastward wind off the geomagnetic equator would produce a westward polarization electric field, which would weaken the EEJ or even reverse the EEJ current. Such a scenario might work for the DE3 climatological winds shown in Figure 1.

To check whether there is any seasonal bias in the data samples used, we carried out a separate analysis of the number of equatorial passes across all longitudes and all seasons for which useful data are available (results not shown here). It is found that the number of equatorial passes is nearly the same for all seasons and there is no bias caused due to data sampling. This reaffirms that the CEJ occurrence pattern observed and reported herein is a genuine feature of the equatorial ionosphere.

It may be noted that the longitudinal dependence of CEJ as could be gleaned from ground data sets is constrained by the data coverage. Marriott et al. (1979) calculated the conditional probability of CEJ occurrence for the various pairs of longitudinally separated stations and found a zonal preference for the CEJ occurrence. In particular, it was suggested that there were more chances of CEJ occurring over two longitudinally separated stations on the same day if it first appeared at the eastern station. This would imply that the CEJ drivers had an influence that extended from east and toward west. It may be seen in Figure 1 that at least for the period of July–September, the preference for the CEJ occurrence is opposite to that suggested by Marriott et al. (1979). In our study, we find that there are more chances of CEJ occurring at a station if it appears earlier in LT to the west of this station. This behavior of the occurrence of CEJ showing preference to the location of the site and time is just a manifestation of the zonal structure and propagation of the DE3 tide.

Recently, Rabiu et al. (2017) revealed the percentage occurrence of CEJ to be higher over Addis Ababa (9.04°N, 38.77°E) than that at Huancayo (12.07°S, 75.22°W). This longitude dependence fits well with the CHAMP observations reported herein. It is also evident from Figure 8 of Rabiu et al. (2017) that the CEJ occurrences at Huancayo and Davao (7°N, 125.58°E) stations are highly diminished during September equinox. Referring to Figure 1, both stations can be seen to lie in the CEJ shadow zones for a range of afternoon LTs.

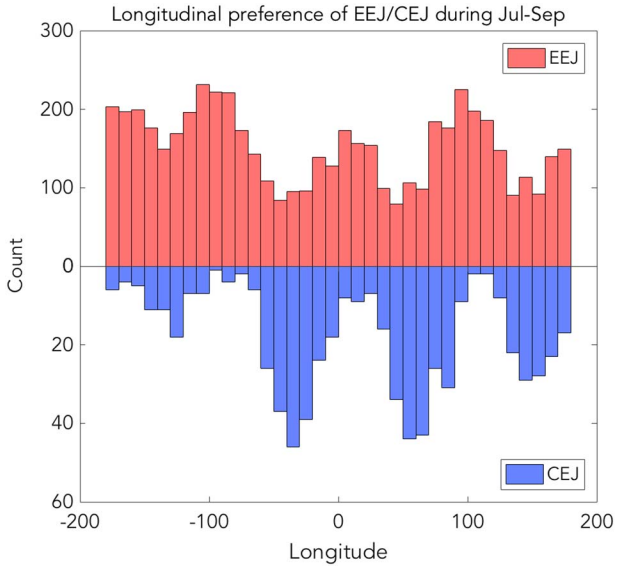

Figure 3. The longitudinal variation of equatorial electrojet (EEJ)/counterelectrojet (CEJ) occurrences showing the complementarity relationship.

Making use of CHAMP observations, McCreadie (2005) identified the preferred longitude zones of occurrence, separately for EEJ and CEJ. Vichare and Rajaram (2011) found CEJ occurrence to be more prominent in longitudes where EEJ is less frequent. This longitudinal complementarity behavior of EEJ and CEJ can be confirmed in Figure 3 where the EEJ/CEJ occurrence rates are depicted for various longitudes for the July–September period. It is now evident that one driver (the DE3 tide, in this case) might facilitate EEJ at some longitudes, while at the same time it might facilitate the occurrence of CEJ at other longitudes. The limited longitudinal extent of CEJ (in the range of 30–60° as reported in the literature; Alex & Mukherjee, 2001; Kane, 1973; Kane & Trivedi, 1981; Rangarajan & Rastogi, 1993; Rastogi, 1974; Vichare & Rajaram, 2011) can be ascribed to one half of the zonal wavelength of the corresponding driving tide(s). For example, stations lying in the CEJ shadow zone during the months of strong DE3 tide would not display a CEJ signature, whereas stations in the adjacent zone (separated over a distance of half a wavelength of the tide (45° for DE3)) would display CEJ signatures.

4. Summary

In this work we present a strong evidence for the influence of DE3 tide on the afternoon CEJ occurrence pattern across the globe. CHAMP magnetometer observations have been used to identify CEJ zones of occurrence. We have also used TIDI zonal wind observations to delineate the longitudinal structure of DE3 tide in a climatological sense. It is readily noted that there is a longitude-LT occurrence pattern of CEJ which is seen to be ordered with respect to the DE3 tide zero-wind line. The four maxima (eastward) and four minima (westward) that describe the DE3 tide longitudinal structure correspond well to the zones of CEJ maximum and minimum occurrence statistics as revealed in the longitude-LT occurrence characteristics depicted in Figure 1. This feature of CEJ occurrence revealed in long-term climatological data is clearly evident during the July–September months when DE3 amplitudes are largest. We have noticed an anomalous behavior of CEJ occurrence in western longitudes, where the dip equator is south of the geographic equator. This may be attributed to the latitudinal structure of DE3 itself, which is known to have maximum amplitudes in southern latitudes, besides the contributions from other nonmigrating tides like DE2.

To conclude, though the DE3 tide with its characteristic peak during July–September months is primarily responsible for the seasonal variation of CEJ at certain longitudes (10–50°W and 50–90°E as can be seen in Figure 2), there could be multiple drivers for the seasonal variation at other longitudes. It is also important to note that the mechanism favoring the occurrence of CEJ over certain longitudes may be favorable to EEJ over certain other longitudes. Modeling efforts can provide further insights of the actual processes underlying the seasonal variation of CEJ in various longitudes.

Acknowledgments
One of the authors, Dupinder Singh (D. S.), would like to thank C. Manoj and Neethal Thomas for useful discussions. A part of this work was carried out during the stay of D. S. at Leibniz Institute of Atmospheric Physics, Germany, under the SCOSTEP Visiting Scholar (SVS) program. The authors gratefully acknowledge the CHAMP and TIDI team for providing the data. The CHAMP data used in this study have been obtained from the Web interface of ISDC at GFZ. TIDI level 3 vector winds can be accessed at ftp://tidi.engin.umich.edu/tidi/vector/. This work is supported by the Department of Science and Technology, Government of India.

References

Alex, S., & Mukherjee, S. (2001). Local time dependence of the equatorial counter electrojet effect in a narrow longitudinal belt. *Earth, Planets and Space*, *53*(12), 1151–1161. https://doi.org/10.1186/BF03352410

Chen, P. R., Luo, Y., & Ma, J. (1995). The QBO modulation of the occurrence of the counter Electrojet. *Geophysical Research Letters*, *22*, 2717–2720. https://doi.org/10.1029/95GL02796

Fejer, B. G., Olson, M. E., Chau, J. L., Stolle, C., Lühr, H., Goncharenko, L. P., & Nagatsuma, T. (2010). Lunar-dependent equatorial ionospheric electrodynamic effects during sudden stratospheric warmings. *Journal of Geophysical Research*, *115*, A00G03. https://doi.org/10.1029/2010JA015273

Finlay, C. C., Olsen, N., Kotsiaros, S., Gillet, N., & Tøffner-clausen, L. (2016). Recent geomagnetic secular variation from Swarm. *Earth, Planets and Space*, *68*(1), 1–18. https://doi.org/10.1186/s40623-016-0486-1

Forbes, J. M., Hagan, M. E., Miyahara, S., Miyoshi, Y., & Zhang, X. (2003). Diurnal nonmigrating tides in the tropical lower thermosphere. *Earth, Planets and Space*, *55*(7), 419–426. https://doi.org/10.1186/BF03351775

Forbes, J. M., Zhang, X., & Bruinsma, S. L. (2014). New perspectives on thermosphere tides: 2. Penetration to the upper thermosphere. *Earth, Planets and Space*, *66*(1), 122. https://doi.org/10.1186/1880-5981-66-122

Gurubaran, S. (2002). The equatorial counter electrojet: Part of a worldwide current system? *Geophysical Research Letters*, *29*(9), 1337. https://doi.org/10.1029/2001GL014519

Hagan, M. E., & Forbes, J. M. (2002). Migrating and nonmigrating diurnal tides in the middle and upper atmosphere excited by tropospheric latent heat release. *Journal of Geophysical Research*, *107*(D24), 4754. https://doi.org/10.1029/2001JD001236

Hagan, M. E., Maute, A., Roble, R. G., Richmond, A. D., Immel, T. J., & England, S. L. (2007). Connections between deep tropical clouds and the Earth's ionosphere. *Geophysical Research Letters*, *114*, L20109. https://doi.org/10.1029/2008JA013637

Hanuise, C., Mazaudier, C., Vila, P., Blanc, M., & Crochet, M. (1983). Global dynamo simulation of ionospheric currents and their connection with the equatorial electrojet and counter electrojet: A case study. *Journal of Geophysical Research: Space Physics*, *88*, 253–270. https://doi.org/10.1029/JA088iA01p00253

He, M., Liu, L., Wan, W., Lei, J., & Zhao, B. (2010). Longitudinal modulation of the O/N2 column density retrieved from TIMED/GUVI measurement. *Geophysical Research Letters*, *37*, L20108. https://doi.org/10.1029/2010GL045105

He, M., Liu, L., Wan, W., & Wei, Y. (2011). Strong evidence for couplings between the ionospheric wave-4 structure and atmospheric tides. *Geophysical Research Letters*, *38*, L14101. https://doi.org/10.1029/2011GL047855

Immel, T. J., Sagawa, E., England, S. L., Henderson, S. B., Hagan, M. E., Mende, S. B., et al. (2006). Control of equatorial ionospheric morphology by atmospheric tides. *Geophysical Research Letters*, *33*, L15108. https://doi.org/10.1029/2006GL026161

Kane, R. P. (1973). *Longitudinal extent of the counter electrojet, Physical Research Laboratory Report AER* (pp. 73–78). Ahmedabad.

Kane, R. P., & Trivedi, N. B. (1981). Confinement of equatorial counter electrojets to restricted longitudes. *Journal of Geomagnetism and Geoelectricity*, *33*(6), 379–382. https://doi.org/10.5636/jgg.33.379

Lühr, H., & Manoj, C. (2013). The complete spectrum of the equatorial electrojet related to solar tides: CHAMP observations. *Annales Geophysicae*, *31*(8), 1315–1331. https://doi.org/10.5194/angeo-31-1315-2013

Lühr, H., & Maus, S. (2006). Direct observation of the *F* region dynamo currents and the spatial structure of the EEJ by CHAMP. *Geophysical Research Letters*, *33*, L24102. https://doi.org/10.1029/2006GL028374

Lühr, H., Maus, S., & Rother, M. (2004). Noon-time equatorial electrojet: Its spatial features as determined by the CHAMP satellite. *Journal of Geophysical Research*, *109*, A01306. https://doi.org/10.1029/2002JA009656

Marriott, R. T., Richmond, A. D., & Venkateswaran, S. V. (1979). The quiet-time equatorial electrojet and counter-electrojet. *Journal of Geomagnetism and Geoelectricity*, *31*(3), 311–340. https://doi.org/10.5636/jgg.31.311

Mayaud, P. N. (1977). The equatorial counter-electrojet—A review of its geomagnetic aspects. *Journal of Atmospheric and Terrestrial Physics*, *39*(9-10), 1055–1070. https://doi.org/10.1016/0021-9169(77)90014-9

McCreadie, H. (2005). Classes of the equatorial electrojet. In *Earth Observation With CHAMP* (pp. 401–406). Berlin, Heidelberg: Springer. https://doi.org/10.1007/3-540-26800-6_64

Oberheide, J., & Forbes, J. M. (2008). Tidal propagation of deep tropical cloud signatures into the thermosphere from TIMED observations. *Geophysical Research Letters*, *35*, L04816. https://doi.org/10.1029/2007GL032397

Onwumechili, A., & Akasofu, S. I. (1972). On the abnormal depression of *Sq*(*H*) under the equatorial electrojet in the afternoon. *Journal of Geomagnetism and Geoelectricity*, *24*(2), 161–173. https://doi.org/10.5636/jgg.24.161

Pedatella, N. M., Forbes, J. M., & Oberheide, J. (2008). Intra-annual variability of the low-latitude ionosphere due to nonmigrating tides. *Geophysical Research Letters*, *35*, L18104. https://doi.org/10.1029/2008GL035332

Rabiu, A. B., Folarin, O. O., Uozumi, T., Hamid, N. S. A., & Yoshikawa, A. (2017). Longitudinal variation of equatorial electrojet and the occurrence of its counter electrojet. *Annales Geophysicae*, *35*(3), 535–545. https://doi.org/10.5194/angeo-35-535-2017

Raghavarao, R., & Anandarao, B. G. (1980). Vertical winds as a plausible cause for equatorial counter electrojet. *Geophysical Research Letters*, *7*, 357–360. https://doi.org/10.1029/GL007i005p00357

Rangarajan, G., & Rastogi, R. G. (1993). Longitudinal difference in magnetic field variations associated with quiet day counter electrojet. *Journal of Geomagnetism and Geoelectricity*, *45*(8), 649–656. https://doi.org/10.5636/jgg.45.649

Rastogi, R. G. (1974). Westward equatorial electrojet during daytime hours. *Journal of Geophysical Research*, *79*, 1503–1512. https://doi.org/10.1029/JA079i010p01503

Reddy, C. A. (1981). The equatorial electrojet: A review of the ionospheric and geomagnetic aspects. *Journal of Atmospheric and Terrestrial Physics*, *43*(5-6), 557–571. https://doi.org/10.1016/0021-9169(81)90118-5

Singh, D., & Gurubaran, S. (2017). Variability of diurnal tide in the MLT region over Tirunelveli (8.7°N), India: Consistency between ground and space based observations. *Journal of Geophysical Research: Atmospheres*, *122*, 2696–2713. https://doi.org/10.1002/2016JD025910

Somayajulu, V. V. (1988). Behavior of harmonic components of the geomagnetic field during counter electrojet events. *Journal of Geomagnetism and Geoelectricity*, *40*(2), 111–130. https://doi.org/10.5636/jgg.40.111

Sridharan, S., Gurubaran, S., & Rajaram, R. (2002). Structural changes in the tidal components in mesospheric winds as observed by the MF radar during afternoon counter electrojet events. *Journal of Atmospheric and Solar-Terrestrial Physics*, *64*(12-14), 1455–1463. https://doi.org/10.1016/S1364-6826(02)00109-8

Stening, R. J., Meek, C. E., & Manson, A. H. (1996). Upper atmosphere wind systems during reverse equatorial electrojet events. *Geophysical Research Letters*, *23*, 3243–3246. https://doi.org/10.1029/96GL02611

Truskowski, A. O., Forbes, J. M., Zhang, X., & Palo, S. E. (2014). New perspectives on thermosphere tides: 1. Lower thermosphere spectra and seasonal-latitudinal structures. *Earth, Planets and Space*, *66*(1), 136. https://doi.org/10.1186/s40623-014-0136-4

Vichare, G., & Rajaram, R. (2011). Global features of quiet time counterelectrojet observed by Ørsted. *Journal of Geophysical Research*, *116*, A04306. https://doi.org/10.1029/2009JA015244

Vineeth, C., Pant, T. K., Devasia, C. V., & Sridharan, R. (2007). Atmosphere-ionosphere coupling observed over the dip equatorial MLTI region through the quasi 16-day wave. *Geophysical Research Letters*, *34*, L12102. https://doi.org/10.1029/2007GL030010

Wan, W., Xiong, J., Ren, Z., Liu, L., Zhang, M. L., Ding, F., et al. (2010). Correlation between the ionospheric WN4 signature and the upper atmospheric DE3 tide. *Journal of Geophysical Research*, *115*, A11303. https://doi.org/10.1029/2010JA015527

Yamazaki, Y., & Maute, A. (2017). Sq and EEJ—A review on the daily variation of the geomagnetic field caused by ionospheric dynamo currents. *Space Science Reviews*, *206*(1-4), 299–405. https://doi.org/10.1007/s11214-016-0282-z

Yamazaki, Y., Richmond, A. D., Maute, A., Liu, H. L., Pedatella, N., & Sassi, F. (2014). On the day-to-day variation of the equatorial electrojet during quiet periods. *Journal of Geophysical Research: Space Physics*, *119*, 6966–6980. https://doi.org/10.1002/2014JA020243